

AI-assisted Early Detection of Pancreatic Ductal Adenocarcinoma on Contrast-enhanced CT

Han Liu*, Riqiang Gao, and Sasa Grbic

Digital Technology and Innovation, Siemens Healthineers

 1st place in the PANORAMA Challenge

Abstract. Pancreatic ductal adenocarcinoma (PDAC) is one of the most common and aggressive types of pancreatic cancer. However, due to the lack of early and disease-specific symptoms, most patients with PDAC are diagnosed at an advanced disease stage. Consequently, early PDAC detection is crucial for improving patients' quality of life and expanding treatment options. In this work, we develop a coarse-to-fine approach to detect PDAC on contrast-enhanced CT scans. First, we localize and crop the region of interest from the low-resolution images, and then segment the PDAC-related structures at a finer scale. Additionally, we develop two strategies to further boost the detection performance, including (1) a data splitting strategy for model ensembling, and (2) a customized post-processing function. We participated in the PANORAMA challenge¹ and ranked 1st place for PDAC detection with an AUROC of 0.9263 and an AP of 0.7243. Our code and models are publicly available at https://github.com/han-liu/PDAC_detection.

Keywords: PDAC, Pancreas Cancer, Early Detection, PANORAMA

1 Introduction

Pancreatic cancer (PAC) is the third most common cause of death due to cancer with a 5-year overall survival of nearly 10% [11,12]. The deadliest type of PAC is pancreatic ductal adenocarcinoma (PDAC), which has been reported to have a 98% loss-of-life expectancy and a 30% increase in the disability-adjusted life years [9]. However, due to the lack of early symptoms, most patients with PDAC are only diagnosed at an advanced stage with disease that is not amenable to curative surgery [10]. If PDAC can be detected at an early stage, the quality of life and treatment options of the patients can be substantially improved [14,13].

Abdominal contrast-enhanced computed tomography (CECT) scan often serves as the first-line diagnostic tool for PDAC detection. Previous studies show that cancer signs, such as pancreatic duct cutoff and atrophy, can be retrospectively identified on CECT scans from 3 to 36 months prior to clinical diagnosis [13,15]. However, early-stage PDAC can be easily overlooked on imaging due

* Corresponding author: han.liu@siemens-healthineers.com

¹ Challenge website: <https://panorama.grand-challenge.org/>

to the subtlety of the tumor and absence of secondary signs [3]. Therefore, it is highly desirable to develop a computer-aided detection system to improve diagnostic accuracy for early PDAC detection.

PANORAMA is the first challenge for PDAC detection with the to-date largest publicly available dataset, providing a standardized platform to develop and evaluate AI models. In this challenge, participants are provided with a training set of portal-venous CECT scans, along with clinical information and segmentation masks for six PDAC-related structures. The objective is to develop an AI algorithm to predict (1) a PDAC detection map, and (2) a patient-level likelihood score. We have participated in the challenge and developed a two-stage PDAC detection method, aiming to segment the target structures in a coarse-to-fine manner. First, we train segmentation models on low-resolution images to efficiently identify the local pancreatic regions. Second, we segment the PDAC-related structures at a finer scale on the cropped regions. Finally, the detection map and the patient-level likelihood are generated based on the segmentation results. Besides, we introduce two strategies that further improve the PDAC detection performance, including (1) a data splitting strategy to create more balanced training sets for model ensembling, and (2) a customized post-processing function to convert segmentation results to detection maps more accurately. Evaluated on the 957 cases from the official testing cohort, our method achieved an AUROC of 0.9263 and an AP of 0.7243 for PDAC detection, ranking 1st overall on the leaderboard.

The rest of this paper is organized as follows. Sec. 2.1 outlines the training pipeline of our PDAC detection framework. Sec. 2.2 and 2.3 introduce two strategies designed to enhance detection performance. Sec. 3.2 reports the results on the official validation and testing cohorts and provide a more in-depth analysis of different training strategies and failure cases on our 5-fold cross validation.

2 Methods

2.1 Two-stage PDAC detection

In most cases, PDAC presents as a single, solid mass on CECT scans. This motivates us to reformulate the PDAC detection task as a segmentation task, where the patient-level likelihood score can be extracted from the segmentation map. Following the challenge baseline algorithm²[1], our proposed method consists of two training stages, aiming to segment PDAC in a coarse-to-fine manner.

In Stage 1, we aim to efficiently identify the local pancreatic regions using low-resolution CECT scans. Specifically, we use the pretrained models from the baseline [1], i.e., 5-fold nnU-Nets [5] that can segment the union of three pancreatic structures: PDAC, pancreas parenchyma, and pancreatic duct. Empirical evaluations confirm that these models are robust enough to crop the region-of-interest (ROI), eliminating the need for retraining. The ROIs are then cropped from the high-resolution images with a margin of $100 \times 50 \times 15$ mm³.

² Baseline: https://github.com/DIAGNijmegen/PANORAMA_baseline

In Stage 2, we train nnU-Nets on the cropped ROIs to segment all six PDAC-related structures. We replace the Dice + Cross entropy (CE) loss with the CE loss to better fit the detection task, and replace the default U-Net architecture with ResU-Net. We use 5-fold cross validation for model selection, with the final segmentation obtained by averaging the softmax probabilities from all folds.

Lastly, we generate the lesion detection map from the segmentation results using the post-processing function in the Report-Guided-Annotation toolkit³ [2]. This function extracts distinct lesion candidates by iteratively identifying the most confident voxels from the softmax probability map of PDAC. Further details are provided in Sec. 2.3. Once the detection map is generated, the final patient-level score is extracted as the maximum value of the detection map.

2.2 Data Splitting Strategy

The distribution of training and validation data is crucial to model generalizability. Prior research in active learning suggests that selecting diverse and representative samples improves learning efficiency [4,16,7]. We extend this principle to the data-splitting process in 5-fold cross validation, ensuring that each fold’s training and validation sets reflect the overall dataset distribution. We consider multiple dataset factors, including lesion size and two clinical variables: age and gender. As shown in Fig. 1, our analyses indicate no strong correlation between gender and PDAC status. While age shows a slight association, it is likely influenced by dataset bias. Lesion size, however, follows a highly skewed distribution among PDAC cases. To achieve balanced representation, we stratify the dataset so that each fold preserves the overall lesion size distribution for PDAC cases. Specifically, we divide lesion sizes into four quartile-based bins (0%, 25%, 50%, 75%, 100%) and maintain the same proportion of samples from each bin across folds. Additionally, we preserve the original PDAC-to-non-PDAC ratio within each fold. This data-splitting strategy allows for models in all folds to be validated on a representative distribution, reducing bias and enhancing generalizability across varying lesion sizes.

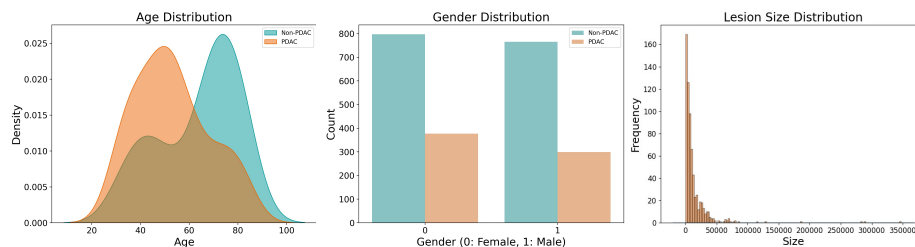


Fig. 1. Age (left), gender (middle), and lesion size (right) distributions of the PANORAMA challenge dataset.

³ Toolkit: <https://github.com/DIAGNijmegen/Report-Guided-Annotation>

2.3 Customized Post-processing

We employ Report-Guided-Annotation [2] to extract the lesion candidates from the segmentation result, i.e., softmax prediction. This method iteratively identifies candidates by starting at the most confident voxel and including all connected voxels exceeding a predefined threshold.

Formally, let $P(x)$ denote the softmax probability map, where x represents a voxel in the 3D image space. The lesion candidate extraction process is defined as follows. First, an initial seed is selected by identifying the voxel with the highest confidence: $x^* = \arg \max_x P(x)$, where x^* denotes the initial seed for the lesion candidate. Second, the candidate region C is expanded by adding all connected voxels x' satisfying: $P(x') \geq \tau$, where τ is the predefined threshold. Third, once the candidate region C is formed, it is removed from the probability map: $P'(x) = P(x) \cdot \mathbb{1}(x \notin C)$, where $P'(x)$ is the updated probability map and $\mathbb{1}(\cdot)$ is an indicator function that excludes voxels in C . This candidate generation process repeats until the desired number of candidates is extracted.

Since τ controls lesion expansion, an inappropriate value can lead to inaccurate detections. By default [1], $\tau = 0.4$, but empirical results indicate that this setting is suboptimal for PDAC detection. To optimize τ , we conduct a grid search on the validation sets using 5-fold cross validation. Since a fixed threshold may not generalize well across all folds, we propose to use an adaptive threshold based on the peak confidence: $\tau = \alpha \cdot P(x^*)$, where α is a scaling factor controlling the expansion relative to the highest confidence voxel. Grid search results indicate that a larger expansion (i.e., smaller α) improves the PDAC detection. In our final submission, we empirically set $\alpha = 1/15$ as detailed later in Fig. 2.

3 Experiments and Results

3.1 Dataset and Evaluation

The challenge dataset consists of ~ 3000 portal-venous contrast-enhanced CT scans, where 2238, 86 (30 lesions), and 957 (323 lesions) cases are used for training, validation, and testing, respectively. AI algorithms are submitted as Docker containers to the challenge platform for evaluation. Two evaluation metrics are used for final ranking, including (1) Area Under Receiver Operating Characteristic (AUROC) for patient-level diagnosis and (2) Average Precision (AP) for lesion-level detection. The final ranking is computed as the average of the rankings based on AUROC and AP.

3.2 Results

Challenge Leaderboard Table 1 presents the validation leaderboard results for the top six teams⁴. Notably, only three teams outperformed the baseline

⁴ <https://panorama.grand-challenge.org/evaluation/development-phase/leaderboard>

Table 1. Validation phase leaderboard (86 cases). **Bold** indicates the best.

| Rank | Team name | AUROC | AP |
|------|---------------|---------------|---------------|
| 1 | DTI (ours) | 0.9750 | 0.8247 |
| | DTI w/o DS | 0.9798 | 0.7983 |
| 2 | FightTumor | 0.9792 | 0.8024 |
| 3 | PANORAMiX | 0.9780 | 0.7620 |
| 4 | Baseline [1] | 0.9714 | 0.7120 |
| 5 | Hero of Ages | 0.9673 | 0.6705 |
| 6 | PanoramaRidge | 0.9452 | 0.6082 |

Table 2. Testing phase leaderboard (957 cases). **Bold** indicates the best.

| Rank | Team name | AUROC | 95% CI | | AP | 95% CI | |
|------|--------------|---------------|---------------|---------------|---------------|---------------|---------------|
| | | | Lower | Upper | | Lower | Upper |
| 1 | DTI (ours) | 0.9263 | 0.9085 | 0.9429 | 0.7243 | 0.6708 | 0.7765 |
| 2 | Hero of Ages | 0.9239 | 0.9068 | 0.9400 | 0.6353 | 0.5780 | 0.6910 |
| 3 | PANORAMiX | 0.9090 | 0.8876 | 0.9288 | 0.7004 | 0.6475 | 0.7517 |
| 4 | FightTumor | 0.9063 | 0.8849 | 0.9263 | 0.6375 | 0.5764 | 0.6965 |
| 4 | DeepMax | 0.9223 | 0.9046 | 0.9390 | 0.6161 | 0.5562 | 0.6736 |
| 4 | Baseline [1] | 0.9223 | 0.9046 | 0.9389 | 0.6335 | 0.5756 | 0.6893 |

method provided by the challenge organizers [1]. The top three teams achieved comparable AUROC scores, whereas our method (Team DTI) attained a significantly higher AP, securing first place overall. To assess the impact of our data-splitting strategy, we also evaluated a variant of our method without it (DTI w/o DS). While this variant yielded a slight improvement in AUROC, it resulted in a substantial decline in AP. Consequently, we submitted the models trained with the data-splitting strategy to the final testing phase. Table 2 presents the testing leaderboard results for the methods that outperform the PANORAMA baseline⁵. Our method achieved an AUROC of 0.9263 and an AP of 0.7243, ranking 1st for both metrics.

Additional Analyses Since the images and the ground truth of the validation set are inaccessible, we conduct extensive experiments using our own 5-fold data split for more in-depth analysis of various training approaches and failure cases. We first investigate the impact of our customized post-processing function, evaluating performance across different values of α . Fig. 2 presents the AP obtained for varying $1/\alpha$ values. For patient-level diagnosis, we observe that the AUROC remains relatively stable across most folds, except for a slight downward trend in folds 3 and 4. For lesion-level detection, AP increases with smaller $1/\alpha$, peaks around 10–15, and declines for larger values. The decrease in AP

⁵ <https://panorama.grand-challenge.org/evaluation/development-phase/leaderboard>

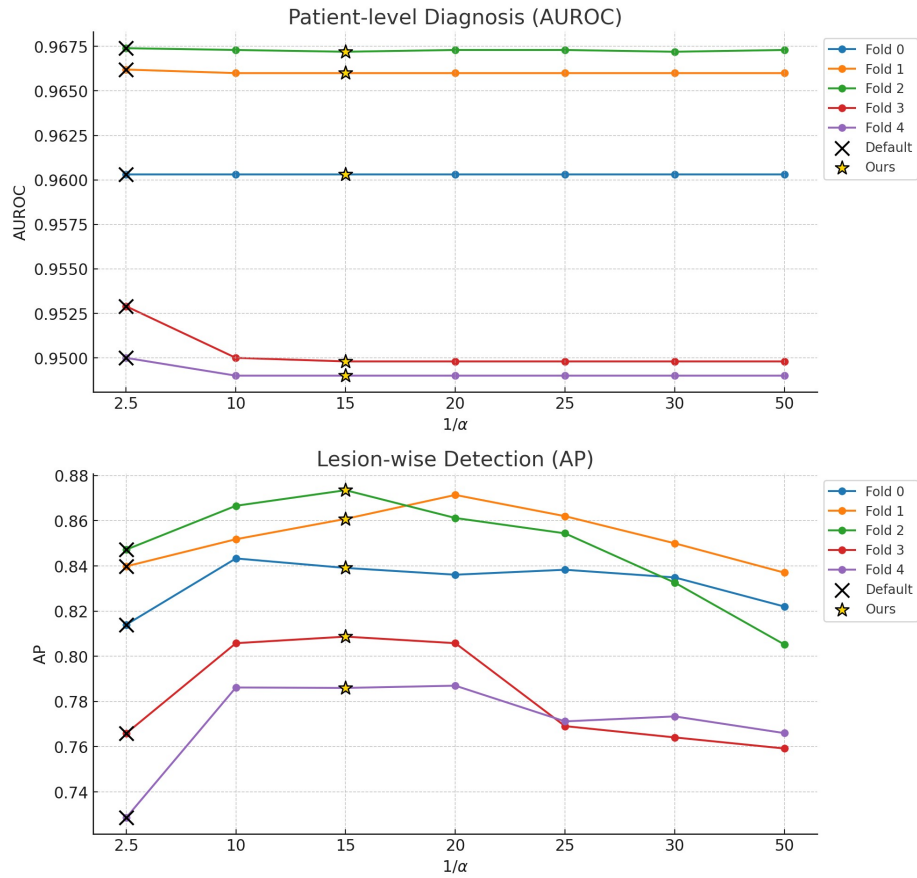


Fig. 2. Impact of α values on the detection results using 5-fold cross validation.

beyond $1/\alpha = 15$ suggests that excessive scaling negatively affects detection performance. Notably, the baseline $\alpha = 0.4$ (denoted by crosses) [1] is suboptimal compared to our optimized α (denoted by stars). Additionally, in folds 3 and 4, AP increases substantially when $1/\alpha$ changes from 2.5 to 10, while AUROC declines, indicating a potential trade-off between the two evaluation metrics in our detection framework.

Furthermore, given the class imbalance observed in Fig. 1, we investigated whether mitigating this imbalance could enhance detection performance. Our approaches included training with weighted cross-entropy loss and oversampling positive samples. Additionally, we experimented with focal loss to emphasize harder cases and implemented a second-stage classifier to reduce false positive predictions. However, none of these strategies yielded improvements in PDAC detection within our experiments.

We conducted a failure case analysis on segmentation results from 5-fold cross-validation, as illustrated in Fig. 3. The figure presents examples of false negatives (left panel) and false positives (right panel). For false negative cases, we observe that PDAC lesions exhibit poorly defined boundaries that make the detection task difficult. In false positive cases, our model struggles to differentiate PDAC from other hypodense pancreatic findings, e.g., multiloculated cystic lesion, leading to misclassifications. These findings underscore the inherent challenges of PDAC detection and highlight the opportunities for further improvement through future research and innovation.

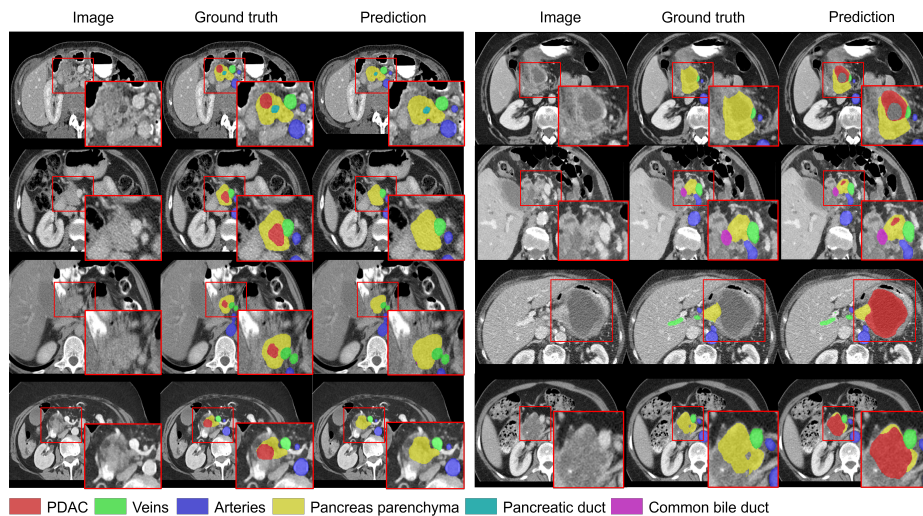


Fig. 3. Examples of failure cases from 5-fold cross validation. **Left panel:** false negative prediction. **Right panel:** false positive prediction.

4 Discussion and Conclusion

In this paper, we propose a two-stage segmentation-based approach for early PDAC detection. To enhance detection performance, we introduce a data-splitting strategy and a customized post-processing function. Evaluated on the challenge testing cohort, our method achieves an AUROC of 0.9263 and an AP of 0.7243, ranking first overall on the leaderboard.

As demonstrated in our failure case analysis, PDAC detection on CECT scans remains highly challenging. Our findings suggest several potential directions for addressing failure cases and improving detection performance. First, since false negative cases exhibit indistinct tumor boundaries on CECT scans, incorporating non-imaging data (e.g., age, sex, and patient history) may provide

more comprehensive and complementary features for early PDAC detection. Second, as PDAC cases with poorly defined tumor boundaries are considered hard samples, it may be beneficial to explore a curriculum learning [6,8] strategy that progressively trains the model from easier to harder cases. Finally, except data splitting based on lesion size, other lesion characteristics, such as PDAC subtypes, could be explored to further improve the model.

Disclaimer. The information in this paper is based on research results that are not commercially available. Future commercial availability cannot be guaranteed.

References

1. Alves, N., Schuurmans, M., Litjens, G., Bosma, J.S., Hermans, J., Huisman, H.: Fully automatic deep learning framework for pancreatic ductal adenocarcinoma detection on computed tomography. *Cancers* **14**(2), 376 (2022)
2. Bosma, J.S., Saha, A., Hosseinzadeh, M., Slootweg, I., de Rooij, M., Huisman, H.: Annotation-efficient cancer detection with report-guided lesion annotation for deep learning-based prostate cancer detection in bpmri. arXiv preprint arXiv:2112.05151 (2021)
3. Elbanna, K.Y., Jang, H.J., Kim, T.K.: Imaging diagnosis and staging of pancreatic ductal adenocarcinoma: a comprehensive review. *Insights into imaging* **11**, 1–13 (2020)
4. Hacothen, G., Dekel, A., Weinshall, D.: Active learning on a budget: Opposite strategies suit high and low budgets. arXiv preprint arXiv:2202.02794 (2022)
5. Isensee, F., Jaeger, P.F., Kohl, S.A., Petersen, J., Maier-Hein, K.H.: nnu-net: a self-configuring method for deep learning-based biomedical image segmentation. *Nature methods* **18**(2), 203–211 (2021)
6. Li, C., Li, M., Peng, C., Lovell, B.C.: Dynamic curriculum learning via in-domain uncertainty for medical image classification. In: *International Conference on Medical Image Computing and Computer-Assisted Intervention*. pp. 747–757. Springer (2023)
7. Liu, H., Li, H., Yao, X., Fan, Y., Hu, D., Dawant, B.M., Nath, V., Xu, Z., Oguz, I.: Colossal: A benchmark for cold-start active learning for 3d medical image segmentation. In: *International Conference on Medical Image Computing and Computer-Assisted Intervention*. pp. 25–34. Springer (2023)
8. Ma, S., Du, H., Curran, K.M., Lawlor, A., Dong, R.: Adaptive curriculum query strategy for active learning in medical image classification. In: *International Conference on Medical Image Computing and Computer-Assisted Intervention*. pp. 48–57. Springer (2024)
9. Michl, P., Löhr, M., Neoptolemos, J.P., Capurso, G., Rebours, V., Malats, N., Ollivier, M., Ricciardiello, L.: Ueg position paper on pancreatic cancer. bringing pancreatic cancer to the 21st century: Prevent, detect, and treat the disease earlier and better. *UEG journal* **9**(7), 860–871 (2021)
10. Park, W., Chawla, A., O’Reilly, E.M.: Pancreatic cancer: a review. *Jama* **326**(9), 851–862 (2021)
11. Schwartz, N.R., Matrisian, L.M., Shrader, E.E., Feng, Z., Chari, S., Roth, J.A.: Potential cost-effectiveness of risk-based pancreatic cancer screening in patients

- with new-onset diabetes. *Journal of the National Comprehensive Cancer Network* **20**(5), 451–459 (2021)
12. Siegel, R.L., Miller, K.D., Jemal, A.: Cancer statistics, 2019. *CA: a cancer journal for clinicians* **69**(1), 7–34 (2019)
 13. Singh, D.P., Sheedy, S., Goenka, A.H., Wells, M., Lee, N.J., Barlow, J., Sharma, A., Kandlakunta, H., Chandra, S., Garg, S.K., et al.: Computerized tomography scan in pre-diagnostic pancreatic ductal adenocarcinoma: Stages of progression and potential benefits of early intervention: A retrospective study. *Pancreatology* **20**(7), 1495–1501 (2020)
 14. Singhi, A.D., Koay, E.J., Chari, S.T., Maitra, A.: Early detection of pancreatic cancer: opportunities and challenges. *Gastroenterology* **156**(7), 2024–2040 (2019)
 15. Toshima, F., Watanabe, R., Inoue, D., Yoneda, N., Yamamoto, T., Sasahira, N., Sasaki, T., Matsuyama, M., Minehiro, K., Tateishi, U., et al.: Ct abnormalities of the pancreas associated with the subsequent diagnosis of clinical stage i pancreatic ductal adenocarcinoma more than 1 year later: a case-control study. *American Journal of Roentgenology* **217**(6), 1353–1364 (2021)
 16. Yehuda, O., Dekel, A., Hacoheh, G., Weinshall, D.: Active learning through a covering lens. *Advances in Neural Information Processing Systems* **35**, 22354–22367 (2022)